



## Utilization of reduced graphene oxide for the enhancement of photocatalytic property of TiO<sub>2</sub> nanotube

Huidi Liu, Yaling Wang, Lei Shi, Ruopeng Xu, Langhuan Huang\*, Shaozao Tan

*Department of Chemistry, Jinan University, Guangzhou 510632, P. R. China, Tel. +86 20 85228817; emails: liuhdjy@163.com (H. Liu), 719658033@qq.com (Y. Wang), 1101465969@qq.com (L. Shi), 289281737@qq.com (R. Xu), Tel./Fax: +86 20 85228817; email: thuanglh@jnu.edu.cn (L. Huang), Tel. +86 20 85223670; email: tanshaozao@163.com (S. Tan)*

Received 12 February 2015; Accepted 25 May 2015

### ABSTRACT

Photocatalysts based on TiO<sub>2</sub> nanotubes and reduced graphene oxide (TNTs-RGO) were prepared by the hydrothermal method. The resulting TNTs-RGO composite photocatalysts were characterized by X-ray powder diffraction, transmission electron microscopy, diffuse reflection spectrum, Fourier transform infrared spectroscopy, N<sub>2</sub> adsorption–desorption isotherm, and fluorescence spectrum. The photocatalytic activity of TNTs-RGO was investigated through the degradation tests of Rhodamine B (RhB) and Cr(VI) under UV-light irradiation. The results showed that compared with TNTs or TiO<sub>2</sub>, TNTs-RGO possessed higher surface area, enhanced optical absorption in the visible-light region and improved separation efficiency of electron–hole pairs, leading to the remarkable increases in adsorption capacity and photocatalytic activity for RhB or Cr(VI), which was thanks to the introduction of RGO. On the basis of the experimental results, a possible photocatalytic degradation mechanism of RhB or Cr(VI) by TNTs-RGO was also proposed. The excellent adsorption capacity and photocatalytic activity suggested the great potential applications of TNTs-RGO photocatalyst in environmental problems.

*Keywords:* TiO<sub>2</sub> nanotube; Reduced graphene oxide; Photocatalytic activity; Adsorption

### 1. Introduction

Titanium dioxide (TiO<sub>2</sub>) has been extensively employed as photocatalyst for solving environmental problems, especially for eliminating pollutants from waste water [1–3]. Photocatalysis process with TiO<sub>2</sub> always suffers from the low quantum yield, which is caused by the rapid recombination of photogenerated electron and hole [4]. Compared with any other forms of TiO<sub>2</sub>, TiO<sub>2</sub> nanotubes (TNTs) have improved properties for various applications in photocatalysis,

sensing and photovoltaics [5–7]. TNTs are of great interest due to their unique tubular structures, size confinements in radial direction and large surface-to-volume ratios [8–10]. Despite the positive attributes, there are also a few defects for TNTs in photocatalysis, which are similar to those of TiO<sub>2</sub> powders or films. In searching for new tools to enhance the photocatalytic activities of semiconductors, graphene-based composites have received significant attention in recent years [11–17]. Graphene with excellent electrical conductivity can be used as an effective electron acceptor to enhance the photoinduced charge transfer [18]. Moreover, graphene has high surface area, which

\*Corresponding author.

could enhance adsorption ability of the graphene-based composite. In addition, the two-dimensional structure makes it possible for graphene-based composite to be synthesized. Recently, many research teams have reported that graphene/TiO<sub>2</sub> nanoparticle can enhance photocatalytic activity in degradations of organic pollutants [14,19], water photocatalytic splitting [20], and antibacterial application [21]. Considering the intrinsic performances of TNTs and graphene, the combination of TNTs with graphene is expected to be an ideal system with superior photocatalytic property [22–24].

Herein, photocatalyst based on TiO<sub>2</sub> nanotubes and reduced graphene oxide (TNTs-RGO) was designed for high-efficiency photocatalytic application. A facile route for preparing TNTs-RGO was developed by the hydrothermal method. The obtained TNTs-RGO composite photocatalyst exhibited remarkably photocatalytic activity for the photocatalytic oxidation of Rhodamine B (RhB) and the photocatalytic reduction of Cr(VI), which could be ascribed to the synergistic effect between TNTs and two-dimensional RGO. Besides, a possible mechanism was proposed to elucidate the role of RGO in TNTs-RGO composite photocatalyst for degradations of pollutants.

## 2. Experimental

### 2.1. Materials

Commercial anatase (TiO<sub>2</sub>, 99%), potassium dichromate (K<sub>2</sub>Cr<sub>2</sub>O<sub>7</sub>, 99.5%), Rhodamine B (RhB, AR), and sodium hydroxide (NaOH, AR) were supplied by Guangzhou Chemical Reagent. All other reagents and solvents were obtained from commercial suppliers. All aqueous solutions were prepared with ultrapure water (>18 MΩ) from a Milli-Q Plus system (Millipore).

### 2.2. Preparation of TNTs

TNTs were synthesized according to the previous report [9]. Briefly, 2.0 g TiO<sub>2</sub> (commercial anatase) was mixed with an aqueous NaOH solution (10 mol/L) in a Teflon vessel at 150°C for 24 h. The resultant products were washed repeatedly with deionized water and diluted HCl and then were calcined at 450°C for 1 h. The obtained powder was designated as TNTs.

### 2.3. Preparation of TNTs-RGO composite photocatalyst

First, graphene oxide (GO) was synthesized from graphite powder by a modified Hummers method [25]. Then, TNTs-RGO composite photocatalysts were

obtained by the hydrothermal method. Briefly, the as-prepared GO was dispersed in 30 mL deionized water. After that, 0.6 g TNTs was added into the above solution. The mixing solution was ultrasonicated for 30 min and vigorously stirred for 3 h to form a stable suspension at room temperature. The weight ratios of GO to TNTs were fixed at 0.0, 1.0, 2.0, and 5.0%, respectively. The homogeneous suspension was transferred into a 50 mL Teflon-lined stainless steel autoclave and held at 120°C for 12 h. After cooling to room temperature, the product was washed with deionized water for several times and then dried under air at 60°C. The obtained samples were denoted as TNTs-RGO composite photocatalysts. Similarly, RGO was prepared according to the same method as described above without the addition of TNTs.

### 2.4. Characterization

The powder X-ray diffraction (XRD) patterns were recorded by an X-ray diffractometer (MSAL-XD II) using a Cu Kα radiation. The transmission electron microscopy (TEM) was performed on a PHILIPS TECNAI-10 microscopy and JEOL JEM-2010 (HR) microscopy. The diffuse reflection spectra (DRS) were determined by a SHIMADZU-2501PC spectrometer equipped with integrating sphere accessory. The fluorescence spectra (FL) were recorded on an F-4500 HITACHI fluorometry. The Fourier transform infrared (FTIR) spectrum was measured by an EQUINOX 55 (Bruker) spectrometer with the KBr pellet technique. The Brunauer–Emmett–Teller (BET) surface area of sample was measured on a Tristar 3000 (Micromeritics) instrument. Nitrogen sorption isotherms were determined by nitrogen adsorption and desorption at 77 K using a surface area and porosimetry system (Micromeritics ASAP 2010). The surface area was calculated using the BET method based on the adsorption.

### 2.5. Adsorption behavior tests

The adsorption tests were carried out using single system containing either RhB or Cr(VI). The adsorption capacity of composite photocatalyst with different content of RGO was performed in a shaker at 25°C. To determine the time required for the adsorption equilibrium of RhB or Cr(VI), 50 mg of composite photocatalyst was added into 100 mL of 10 mg/L target compound solution. Moreover, Cr(VI) system was performed at pH 2. The saturated adsorption amount  $q_e$  (mg/g) was calculated according to the following Eq. (1):

$$q_e = \frac{V \times (C_0 - C_e)}{m} \quad (1)$$

where  $V$  was the volume of target compound solution,  $m$  was the mass of composite photocatalyst,  $C_0$  was the initial concentration, and  $C_e$  was the equilibrium concentration.

### 2.6. Photocatalytic experiments

Photocatalytic experiments were performed in a XUJIANG XPA-II photochemistry reactor. A 500-W high-pressure UVA bulb with the maximal emission at 365 nm was used as light source. The reaction suspension was prepared by adding 50 mg of composite photocatalyst into 100 mL of 10 mg/L target compound solution. Prior to photocatalytic experiment, the suspension was magnetically stirred in a dark for 1 h to establish an adsorption and desorption equilibrium. Cr(VI) system was performed at pH 2. The concentrations of RhB and Cr(VI) solution were quantified by a TU-1900 spectrophotometer at 551 and 349 nm, respectively.

## 3. Results and discussion

### 3.1. XRD, FTIR, and Raman analysis

Fig. 1 showed the XRD patterns of  $\text{TiO}_2$  and TNTs-RGO composite photocatalysts with different contents of RGO. As shown, the peaks at  $25.3^\circ$ ,  $37.8^\circ$ ,  $48.0^\circ$ ,  $53.8^\circ$ ,  $54.9^\circ$ , and  $62.5^\circ$  were the diffractions of (1 0 1), (0 0 4), (2 0 0), (1 0 5), (2 1 1), and (2 0 4) planes of anatase, respectively. It was clearly seen that the XRD patterns of TNTs-RGO samples almost coincided with that of pure  $\text{TiO}_2$ . However, no typical diffraction peak of GO or RGO was observable in the XRD patterns for TNTs-RGO samples. On one hand, this might

be due to the low level of GO or RGO. On the other hand, this might be ascribed to the fact that GO could be reduced to RGO during the hydrothermal reaction [15] and the strong diffraction peak of anatase at  $25.3^\circ$  could cover the peak of RGO at  $24.5^\circ$  [26]. Furthermore, FTIR was also performed to illustrate a successful reduction of GO to RGO by hydrothermal reaction. Fig. 2 showed the FTIR spectra of the as-prepared GO and TNTs-2.0%RGO. For GO, the peaks at 1,721, 1,630, 1,407, 1,223, and 1,048  $\text{cm}^{-1}$ , respectively, corresponded to C=O, C=C, alcoholic C–O, phenolic C–OH and C–O vibration frequencies, confirming the presences of various oxygen-functional groups in GO. Compared with GO, the intensities of typical absorption bands of oxygen-functional groups decreased significantly in TNTs-2.0%RGO, indicating that GO had been successfully reduced to RGO. Moreover, the strong band at 495  $\text{cm}^{-1}$  was ascribed to the Ti–O stretching vibration of  $\text{TiO}_2$ .

In the Raman spectra (Fig. 3), both of the curves exhibited two peaks at 1,340 and 1,580  $\text{cm}^{-1}$ , corresponding to the characteristic D and G bands of graphitic material, respectively. Generally speaking, the intensity ratio of the D band and G band ( $I_D/I_G$ ) could be used to roughly estimate the average size of the  $\text{sp}^2$  domain of the graphite material. It was found that  $I_D/I_G$  value of GO (1.25) was higher than that of TNTs-2.0%RGO (1.10), which indicated that the  $\pi$ -conjugated structure from GO was recovered after hydrothermal reduction. Such results were consistent with FITR results.

### 3.2. TEM analysis

The TEM images of RGO, TNTs, and TNTs-2.0% RGO were shown in Fig. 4. In Fig. 4(a), the

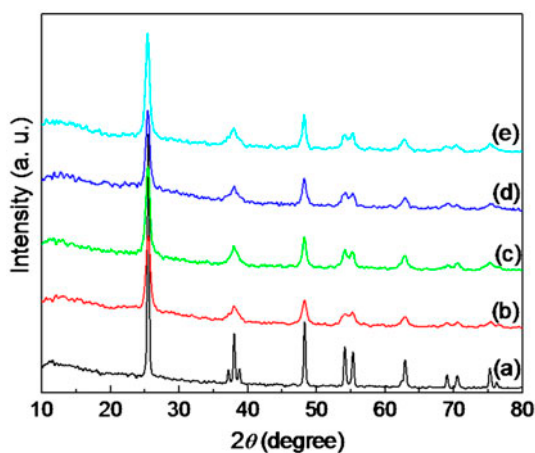


Fig. 1. XRD patterns of (a)  $\text{TiO}_2$ , (b) TNTs, (c) TNTs-1.0% RGO, (d) TNTs-2.0%RGO and (e) TNTs-5.0%RGO.

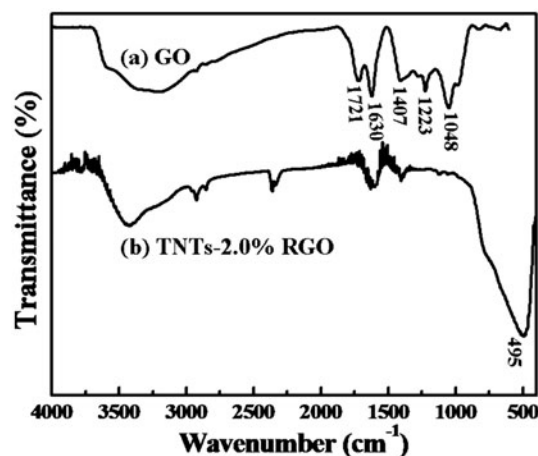


Fig. 2. FTIR spectra of (a) GO and (b) TNTs-2.0%RGO.

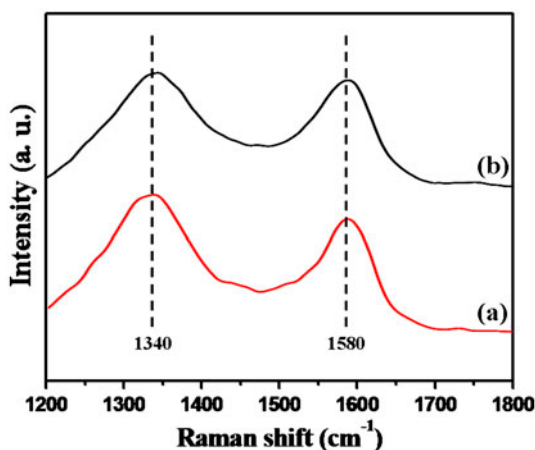


Fig. 3. Raman spectra of (a) GO and (b) TNTs-2.0%RGO.

morphology of RGO was observed clearly, which showed that RGO was highly transparent with some visible wrinkles and ripples. Fig. 4(b) showed the tubular morphologies of TNTs and the TNTs seemed to have agglomeration in a way. However, with the introduction of RGO, the agglomeration of TNTs had been reduced, indicating that RGO could make the

TNTs disperse well in aqueous solution (Fig. 4(c)). Furthermore, the HRTEM of TNTs-2.0%RGO was observed in Fig. 4(d). As seen, TNTs closely touched with RGO, which made the electronic interaction between TNTs and RGO possible, leading to the enhancement of charge separation and photocatalytic activity [27]. Besides, the interlayer space was approximately 0.35 nm, corresponding to the spacing of the (1 0 1) plane of  $\text{TiO}_2$ . The selected area electron diffraction patterns (SAED) also proved it.

### 3.3. BET analysis

In general, the surface area of photocatalyst was an important factor for influencing the photocatalytic activity of photocatalyst [28,29]. The surface areas of all samples were shown in Table 1. All TNTs-RGO composite photocatalysts had higher BET surface area than  $\text{TiO}_2$ . Such results might be ascribed that the introduction of RGO with high BET surface area, which could effectively prevent TNTs from agglomeration and consequently had significant effect on the BET surface area of composite photocatalyst. The surface area of the TNTs-5.0%RGO composite

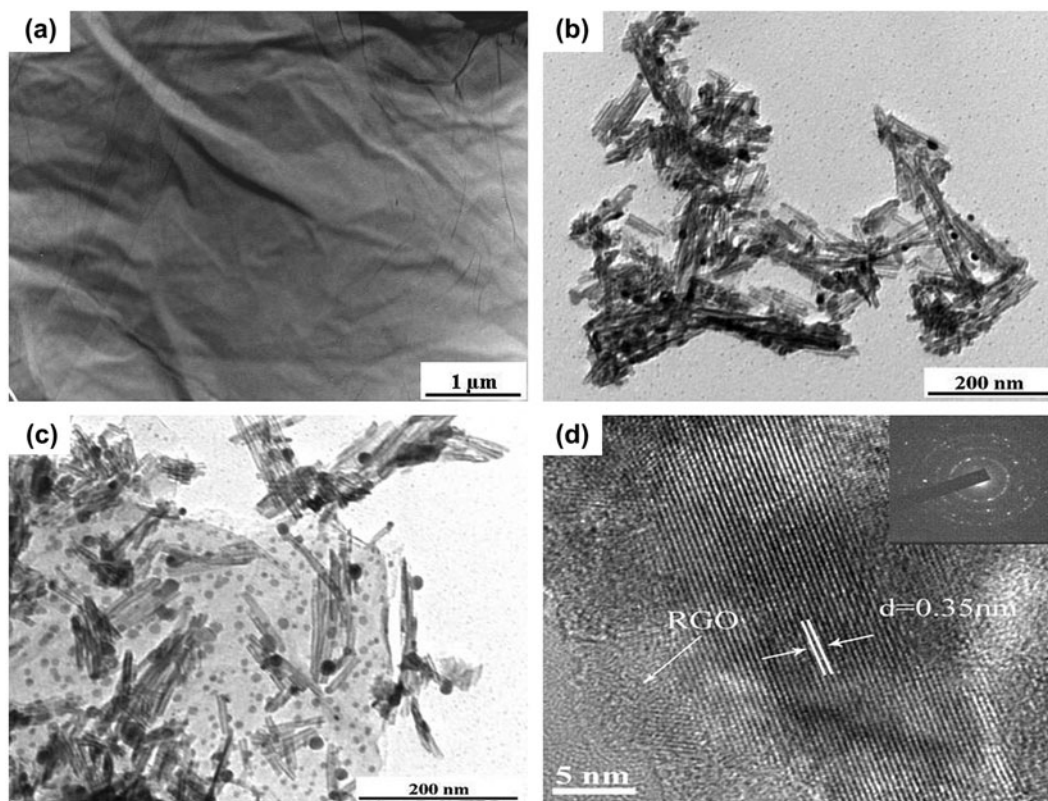


Fig. 4. TEM images of (a) RGO, (b) TNTs and (c) TNTs-2.0%RGO; (d) HRTEM image of TNTs-2.0%RGO.

Table 1  
Summary of the characterization results for different photocatalysts

Photocatalysts	$S_{\text{BET}}$ ( $\text{m}^2/\text{g}$ )	Adsorption kinetic constants (RhB)			Adsorption kinetic constants (Cr)		
		$q_e$ (mg/g)	$K_a$ (L/mg)	$R^2$	$q_e$ (mg/g)	$K_a$ (L/mg)	$R^2$
RGO	331	–	–	–	–	–	–
TiO <sub>2</sub>	11.1	1.048	0.1267	0.988	0.413	2.4154	0.997
TNT	107	1.803	0.0498	0.987	0.592	0.1841	0.992
TNT-1.0%RGO	119	4.627	0.1103	0.999	1.105	0.0813	0.996
TNT-2.0%RGO	121	7.340	0.0327	0.996	1.189	0.1951	0.998
TNT-5.0%RGO	286	14.05	0.0137	0.997	1.668	0.1704	0.998

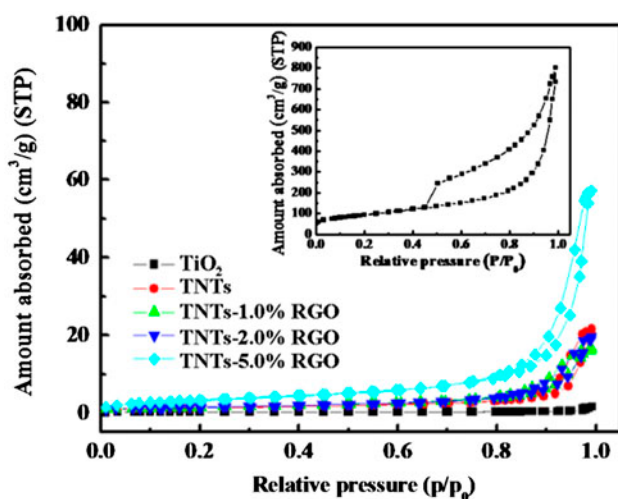


Fig. 5. The N<sub>2</sub> adsorption–desorption isotherms for TiO<sub>2</sub> and TNTs-RGO composite photocatalysts (inset was the N<sub>2</sub> adsorption–desorption isotherm for RGO).

photocatalyst was nearly 26 times as large as that of TiO<sub>2</sub> and 3 times as large as that of TNTs. It was observed that the surface area increased with the increase of RGO content in the TNTs-RGO sample. Photocatalyst with higher specific surface would supply more surface active sites and enhance charge transportation, which would improve the photocatalytic activity [16]. The nitrogen adsorption–desorption isotherms for TiO<sub>2</sub>, RGO, and TNTs-RGO photocatalysts were shown in Fig. 5.

### 3.4. Adsorption behavior

The adsorption kinetics of RhB or Cr(VI) was studied according to the pseudo-second-order model, which could be expressed as follows:

$$\frac{t}{q_t} = \frac{1}{kq_e^2} + \frac{t}{q_e} \quad (2)$$

where  $k$  (mg/g min) was the rate constant of the pseudo-second-order adsorption;  $q_e$  (mg/g) and  $q_t$  (mg/g) were, respectively, the quantities of target compound adsorbed at equilibrium and at any time. Fig. 6 showed the adsorption capacity vs. the adsorption time for RhB or Cr(VI) by TNTs-RGO sample. The adsorption kinetics of RhB or Cr(VI) was shown in Fig. 7. The obtained parameters were presented in Table 1. The good linear relationship for target compound indicated that the adsorption conformed to pseudo-second-order kinetics. It could be clearly seen that the adsorption of target compound was quite rapid during the first 20 min. Thereafter, it proceeded at a lower rate and finally attained saturation. The necessary time to reach the equilibrium was about 1 h and increasing the removal time to 4 h did not show notable effect. At equilibrium, the amounts of RhB and Cr(VI) adsorbed onto the TNTs-RGO sample increased from 1.803 to 14.05 mg/g and from 0.4132 to 1.668 mg/g, respectively, as the RGO content increased from 0 to 5.0%. Compared with the pure TNTs counterpart, TNTs-RGO samples had higher specific area. Therefore, the improvement in adsorption capacity as increasing the RGO content could be attributed to the increase of specific area.

### 3.5. DRS and PL analysis

Also, the optical property was a factor in determining the photocatalytic activity of photocatalyst. The diffuse reflectance UV–vis spectra of TiO<sub>2</sub> and TNTs-RGO samples with different contents of RGO were presented in Fig. 8. It was evident that pure TiO<sub>2</sub> and TNTs had no adsorption in the visible-light region (>400 nm). However, the introduction of RGO significantly affected the absorption property of the composite photocatalyst. For TNTs-RGO samples, the optical absorptions in the visible-light region were enhanced. In addition, it was noticeable that there was an obvious correlation between the RGO content and the

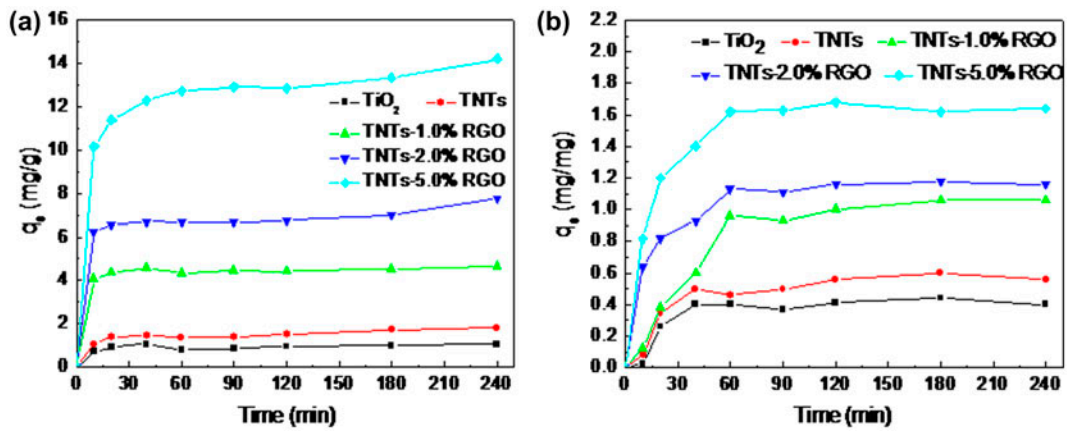


Fig. 6. The adsorption capacity vs. the adsorption time of (a) RhB and (b) Cr(VI).

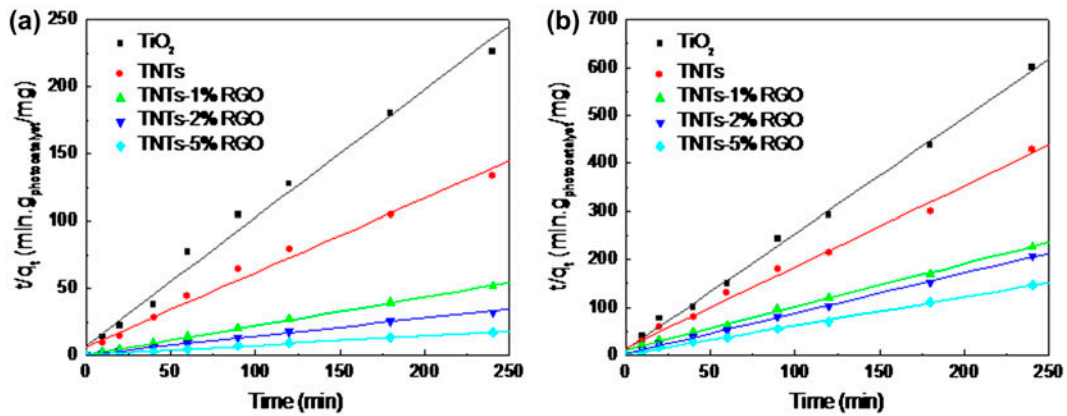


Fig. 7. The adsorption kinetics of (a) RhB and (b) Cr(VI) by TNTs-RGO composite photocatalysts.

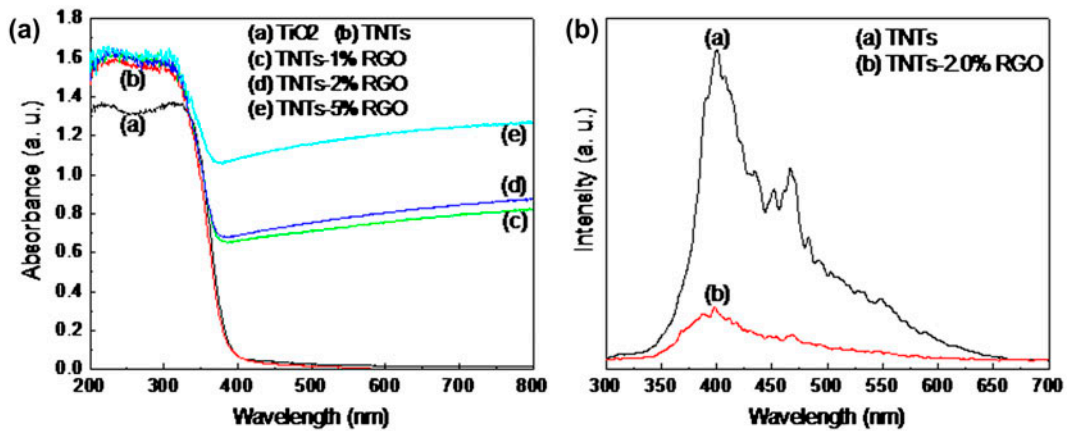


Fig. 8. The diffuse reflectance UV-vis spectra of  $\text{TiO}_2$  and TNTs-RGO composite photocatalysts (Left). The PL intensity of TNTs and TNTs-2.0%RGO (Right).

change of UV–vis spectrum. The enhancement of absorption in the visible-light region increased with the increase of RGO content. Also, there were red shifts of the adsorption edges of TNTs-RGO samples compared with that of pure TNTs. As shown in Fig. 8, the PL intensity of TNTs-2.0%RGO was much lower than that of pure TNTs. As known, the PL signal was attributed to the radiative recombination process of self-trapped exciton [30]. Thus, the decrease of PL intensity indicated the enhancement of separation efficiency of electron–hole pairs. The experimental results demonstrated that the separation efficiency of electron–hole pairs was quite sensitive to the content of RGO. Thus, RGO might play an important role in improving the photocatalytic activity.

### 3.6. Photocatalytic reaction

The photocatalytic efficiency was evaluated by the photocatalytic oxidation of RhB or the photocatalytic reduction of Cr(VI) in an aqueous solution under UV-light irradiation. Fig. 9(a) showed the photocatalytic oxidation results for RhB over various TNTs-RGO samples. For comparison, bare TNTs and TiO<sub>2</sub> were used as reference. Under UV-light irradiation, all TNTs-RGO had high photocatalytic activity, which was apparently caused by photocatalytic oxidation process. An approximate 97% of the RhB was removed by TNT-5%RGO sample within 10 min, whereas only 68% of the RhB was degraded by bare TNTs during the same time duration. With the increase of RGO content, the photocatalytic activities of TNTs-RGO samples were improved monotonously. The corresponding degradation rate constants of TiO<sub>2</sub>, TNTs, TNTs-1.0%RGO, TNTs-2.0%RGO, and TNTs-5.0%RGO were estimated to be 0.0897, 0.117,

0.142, 0.294, and 0.413 min<sup>-1</sup>, respectively. The sample with 5.0% RGO showed the highest photocatalytic activity, which was up to 4 times than that of TiO<sub>2</sub> and 3 times than that of TNTs. Fig. 9(b) showed the photocatalytic reduction results for Cr(VI) over various TNTs-RGO samples. Similarly, all TNTs-RGO had definite photocatalytic activity under UV-light irradiation, which was obviously caused by photocatalytic reduction process. The results showed that the photocatalytic activity of composite increased with the TNTs-RGO ratio increased initially. However, the photocatalytic activity of composite decreased when RGO content exceeded 2.0 wt%. The corresponding degradation rate constants of TiO<sub>2</sub>, TNTs, TNTs-1.0%RGO, TNTs-2.0%RGO, and TNTs-5.0%RGO were estimated to be 0.00255, 0.0118, 0.0145, 0.0191, and 0.0127 min<sup>-1</sup>, respectively. Compared to the photocatalytic oxidation of RhB, the degradation rate constants for Cr(VI) reduction were lower. The reason was that the photoreaction in a completely inorganic solution included simultaneous reduction of Cr(VI) to Cr(III) with oxidation of O<sup>2-</sup> to O<sub>2</sub>, and the production of O<sub>2</sub> was a slow four-electron process [31,32], which resulted in a poor photocatalytic performance. However, the results of photocatalytic reduction for Cr(VI) also showed that the sample with 2.0% RGO exhibited the highest photocatalytic activity, which was up to 7 times than that of TiO<sub>2</sub> and nearly 2 times than that of TNTs. All experimental results demonstrated that TNTs-RGO samples had much higher photocatalytic activities than bare TNTs for the disposal of Cr(VI) and especially for the disposal of RhB. A plot of  $-\ln(C_t/C_0)$  vs.  $t$  for RhB or Cr(VI) degradation with different photocatalysts was presented in Fig. 10. The parameters obtained were presented in Table 2.

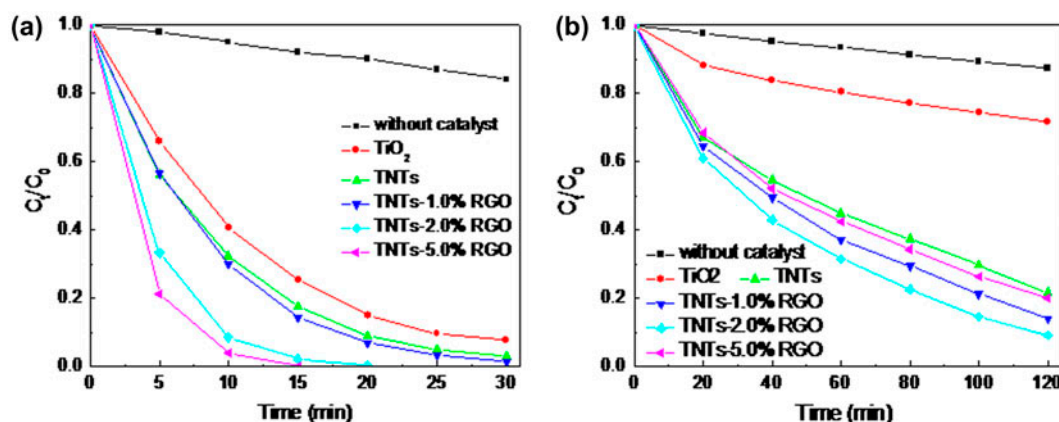


Fig. 9. Photocatalytic degradation of (a) RhB and (b) Cr(VI) by TNTs composite photocatalyst under UV-light irradiation.

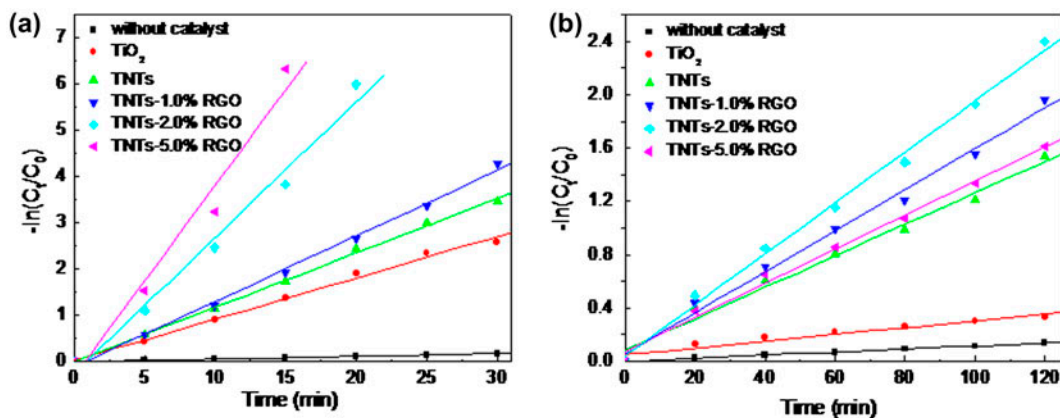


Fig. 10. The degradation kinetics of (a) RhB and (b) Cr(VI) by TNTs-RGO composite photocatalysts.

Table 2  
Parameters of pseudofirst-order kinetics for RhB and Cr(VI)

Photocatalysts	Kinetic constants		Kinetic constants	
	$K_{app}$ ( $\text{min}^{-1}$ )	$R^2$	$K_{app}$ ( $\text{min}^{-1}$ )	$R^2$
Without photocatalyst	0.00582	0.995	0.00112	0.998
TiO <sub>2</sub>	0.0897	0.994	0.00255	0.938
TNTs	0.117	0.998	0.0118	0.986
TNTs-1.0%RGO	0.142	0.996	0.0154	0.991
TNTs-2.0%RGO	0.294	0.983	0.0191	0.991
TNTs-5.0%RGO	0.413	0.969	0.0127	0.992

### 3.7. Photocatalytic mechanism

For the photocatalytic degradation of RhB and the photocatalytic reduction of Cr(VI), both mechanisms were different. For the former, the RhB molecule was oxidized by photogenerated hole and OH which was produced by the combination of hole and water or hydroxyl group. Thus, the RhB molecule could be photocatalytically decomposed to CO<sub>2</sub> and H<sub>2</sub>O. For

the latter, the reduction of Cr(VI) to Cr(III) was influenced by the photogenerated electron. Therefore, the separation ratio of photogenerated electron-hole pair was quite important in both photodegradation of RhB and photoreduction of Cr(VI). Compared with that of TNTs, the enhanced photocatalytic performance of TNTs-RGO could be ascribed to the excellent electronic transmission property of RGO, which acted as

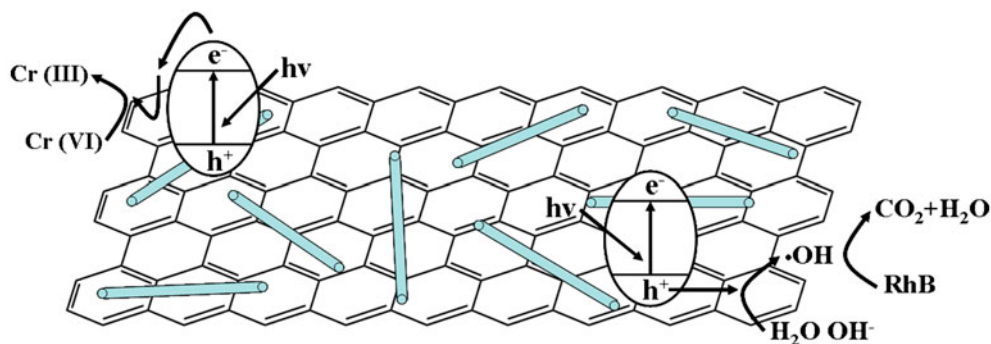


Fig. 11. The schematic illustration of the photocatalytic mechanism of RhB and Cr(VI) by TNTs-RGO.

an electron acceptor and effectively suppressed the recombination of photogenerated electron–hole pair (as shown in Fig. 11).

#### 4. Conclusions

TNTs-RGO composite photocatalysts had been prepared in this study. Comparison of all experimental results showed that TNTs-RGO samples had higher photocatalytic than TNTs. The reasons could be explained as follows: (1) Adsorption behavior tests showed that compared with TNTs, TNTs-RGO samples possessed better adsorption properties, which was because TNTs-RGO samples possessed higher surface areas. This could supply more surface active sites and enhance charge transportation; (2) the DRS analysis demonstrated that TNTs-RGO samples could absorb more visible light compared with TNTs; (3) the FL analysis indicated that the introduction of RGO was helpful to increase the separation efficiency of electron–hole pair. From these three aspects, TNTs-RGO samples could enhance photocatalytic activity greatly. We also confirmed that TNTs-RGO samples could have not only photocatalytic oxidation of RhB, but also photocatalytic reduction of Cr(VI) in an aqueous solution under UV-light irradiation. Thus, TNTs-RGO composite photocatalysts would have a wide range of application in photocatalytic field.

#### Acknowledgments

The authors acknowledge financial support from the National Natural Science Foundation of China (21476052 and 21271087) and the Foundation of Enterprise-University-Research Institute Cooperation from Guangdong Province and the Ministry of Education of China (2013B090600148).

#### References

- [1] L.H. Huang, Q.Z. Chan, X.J. Wu, H.J. Wang, Y.L. Liu, The simultaneous photocatalytic degradation of phenol and reduction of Cr(VI) by TiO<sub>2</sub>/CNTs, *J. Ind. Eng. Chem.* 18 (2012) 574–580.
- [2] S.K. Lee, A. Mills, Detoxification of water by semiconductor photocatalysis, *J. Ind. Eng. Chem.* 10 (2004) 173–187.
- [3] P. Roy, S. Berger, P. Schmuki, TiO<sub>2</sub> nanotubes: Synthesis and applications, *Angew. Chem. Int. Ed.* 50 (2011) 2904–2939.
- [4] T. Berger, M. Sterrer, O. Diwald, E. Knözinger, D. Panayotov, T.L. Thompson, J.T. Yates, Light-induced charge separation in anatase TiO<sub>2</sub> particles, *J. Phys. Chem. B* 109 (2005) 6061–6068.
- [5] W.L. Xue, G.W. Zhang, X.F. Xu, X.L. Yang, C.J. Liu, Y.H. Xu, Preparation of titania nanotubes doped with cerium and their photocatalytic activity for glyphosate, *Chem. Eng. J.* 167 (2011) 397–402.
- [6] M.H. Seo, M. Yuasa, T. Kida, J.S. Huh, K. Shimano, N. Yamazoe, Gas sensing characteristics and porosity control of nanostructured films composed of TiO<sub>2</sub> nanotubes, *Sens. Actuators B* 137 (2009) 513–520.
- [7] T. Rattanavoravipa, T. Sagawa, S. Yoshikawa, Photovoltaic performance of hybrid solar cell with TiO<sub>2</sub> nanotubes arrays fabricated through liquid deposition using ZnO template, *Sol. Energy Mater. Sol. Cells* 92 (2008) 1445–1449.
- [8] L.H. Huang, C. Sun, Y.L. Liu, Pt/N-codoped TiO<sub>2</sub> nanotubes and its photocatalytic activity under visible light, *Appl. Surf. Sci.* 253 (2007) 7029–7035.
- [9] T. Kasuga, M. Hiramatsu, A. Hoson, T. Sekino, K. Niihara, Formation of titanium oxide nanotube, *Langmuir* 14 (1998) 3160–3163.
- [10] Q. Chen, W.Z. Zhou, G.H. Du, L.M. Peng, Trititanate nanotubes made via a single alkali treatment, *Adv. Mater.* 14 (2002) 1208–1211.
- [11] Q.J. Xiang, J.G. Yu, M. Jaroniec, Preparation and enhanced visible-light photocatalytic H<sub>2</sub>-production activity of graphene/C<sub>3</sub>N<sub>4</sub> composites, *J. Phys. Chem. C* 115 (2011) 7355–7363.
- [12] G.D. Jiang, Z.F. Lin, C. Chen, L.H. Zhu, Q. Chang, N. Wang, W. Wei, H.Q. Tang, TiO<sub>2</sub> nanoparticles assembled on graphene oxide nanosheets with high photocatalytic activity for removal of pollutants, *Carbon* 49 (2011) 2693–2701.
- [13] Y.F. Sun, B.Y. Qu, Q. Liu, S. Gao, Z.X. Yan, W.S. Yan, B.C. Pan, S.Q. Wei, Y. Xie, Highly efficient visible-light-driven photocatalytic activities in synthetic ordered monoclinic BiVO<sub>4</sub> quantum tubes-graphene nanocomposites, *Nanoscale* 4 (2012) 3761–3767.
- [14] T.D. Nguyen-Phan, V.H. Pham, E.W. Shin, H.D. Pham, S. Kim, J.S. Chung, E.J. Kim, S.H. Hur, The role of graphene oxide content on the adsorption-enhanced photocatalysis of titanium dioxide/graphene oxide composites, *Chem. Eng. J.* 170 (2011) 226–232.
- [15] Y.H. Zhang, Z.R. Tang, X.Z. Fu, Y.J. Xu, TiO<sub>2</sub>-graphene nanocomposites for gas-phase photocatalytic degradation of volatile aromatic pollutant: Is TiO<sub>2</sub>-graphene truly different from other TiO<sub>2</sub>-carbon composite materials? *ACS Nano* 4 (2010) 7303–7314.
- [16] Q. Li, B.D. Guo, J.G. Yu, J.R. Ran, B.H. Zhang, H.J. Yan, J.R. Gong, Highly efficient visible-light-driven photocatalytic hydrogen production of cds-cluster-decorated graphene nanosheets, *J. Am. Chem. Soc.* 133 (2011) 10878–10884.
- [17] J.G. Radich, A.L. Krenselewski, J.D. Zhu, P.V. Kamat, Is graphene a stable platform for photocatalysis? Mineralization of reduced graphene oxide with UV-irradiated TiO<sub>2</sub> nanoparticles, *Chem. Mater.* 26 (2014) 4662–4668.
- [18] R. Sellappan, J. Sun, A. Galeckas, N. Lindvall, A. Yurgens, A.Y. Kuznetsov, D. Chakarov, Influence of graphene synthesizing techniques on the photocatalytic performance of graphene-TiO<sub>2</sub> nanocomposites, *Phys. Chem. Chem. Phys.* 15 (2013) 15528–15537.
- [19] S. Umrao, S. Abraham, F. Theil, S. Pandey, V. Ciobotă, P.K. Shukla, C.J. Rupp, S. Chakraborty, R. Ahuja, J. Popp, B. Dietzek, A. Srivastava, A possible mechanism

- for the emergence of an additional band gap due to a Ti–O–C bond in the TiO<sub>2</sub>-graphene hybrid system for enhanced photodegradation of methylene blue under visible light, *RSC Adv.* 4 (2014) 59890–59901.
- [20] X.Y. Zhang, H.P. Li, X.L. Cui, Y.H. Lin, Graphene/TiO<sub>2</sub> nanocomposites: Synthesis, characterization and application in hydrogen evolution from water photocatalytic splitting, *J. Mater. Chem.* 20 (2010) 2801–2806.
- [21] O. Akhavan, E. Ghaderi, Photocatalytic reduction of graphene oxide nanosheets on TiO<sub>2</sub> thin film for photoinactivation of bacteria in solar light Irradiation, *J. Phys. Chem. C* 113 (2009) 20214–20220.
- [22] Q.Q. Zhai, T. Bo, G.X. Hu, High photoactive and visible-light responsive graphene/titanate nanotubes photocatalysts: Preparation and characterization, *J. Hazard. Mater.* 198 (2011) 78–86.
- [23] S.D. Perera, R.G. Mariano, K. Vu, N. Nour, O. Seitz, Y. Chabal, K.J. Balkus, Hydrothermal synthesis of graphene-TiO<sub>2</sub> nanotube composites with enhanced photocatalytic activity, *ACS Catal.* 2 (2012) 949–956.
- [24] S.D. Perera, R.G. Mariano, K. Vu, N. Nour, O. Seitz, Y. Chabal, K.J. Balkus, Hydrothermal synthesis of graphene-TiO<sub>2</sub> nanotube composites with enhanced photocatalytic activity, *ACS Catal.* 2 (2012) 949–956.
- [25] W.S. Hummers, R.E. Offeman, Preparation of graphitic oxide, *J. Am. Chem. Soc.* 80 (1958) 1339–1339.
- [26] Y.J. Xu, Y.B. Zhuang, X.Z. Fu, New insight for enhanced photocatalytic activity of TiO<sub>2</sub> by doping carbon nanotubes: A case study on degradation of benzene and methyl orange, *J. Phys. Chem. C* 114 (2010) 2669–2676.
- [27] F. Zhou, R. Shi, Y.F. Zhu, Significant enhancement of the visible photocatalytic degradation performances of  $\gamma$ -Bi<sub>2</sub>MoO<sub>6</sub> nanoplate by graphene hybridization, *J. Mol. Catal. A-Chem.* 340 (2011) 77–82.
- [28] N. Sobana, M. Muruganadham, M. Swaminathan, Nano-Ag particles doped TiO<sub>2</sub> for efficient photodegradation of direct azo dyes, *J. Mol. Catal. A-Chem.* 258 (2006) 124–132.
- [29] M. Moonsiri, P. Rangsunvigit, S. Chavadej, E. Gulari, Effects of Pt and Ag on the photocatalytic degradation of 4-chlorophenol and its by-products, *Chem. Eng. J.* 97 (2004) 241–248.
- [30] L.H. Huang, H.J. Wang, Y.L. Liu, C.X. Chen, Preparation, characterization and photocatalytic activity of Pt-SiO<sub>2</sub>/TiO<sub>2</sub> with core-shell structure, *Rare Metal Mater. Eng.* 11 (2011) 1901–1905.
- [31] C. Wang, M.H. Cao, P.F. Wang, Y.H. Ao, J. Hou, J. Qian, Preparation of graphene-carbon nanotube-TiO<sub>2</sub> composites with enhanced photocatalytic activity for the removal of dye and Cr(VI), *Appl. Catal. A-Gen.* 473 (2014) 83–89.
- [32] N. Wang, Y.Z. Xu, L.H. Zhu, X.T. Shen, H.Q. Tang, Reconsideration to the deactivation of TiO<sub>2</sub> catalyst during simultaneous photocatalytic reduction of Cr(VI) and oxidation of salicylic acid, *J. Photoch. Photobio. A* 201 (2009) 121–127.